High-Gradient Magnetic Separator (HGMS) combined with adsorption for Nitrate removal from aqueous solution

Z. Kheshti [1], K. Azodi Ghajar[2], Ali Altaee* [3], M. R. Kheshti[2]

[1]Department of Chemical Engineering, School of Chemical and Petroleum Engineering, Shiraz University, Shiraz 7193616511, Iran.

[2]Department of Mechanical Engineering, Shiraz University, Shiraz 7193616548, Iran.

[3]School of Civil and Environmental Engineering, University of Technology Sydney, Ultimo, NSW 2007, Australia

* Ali.Altaee@uts.edu.au

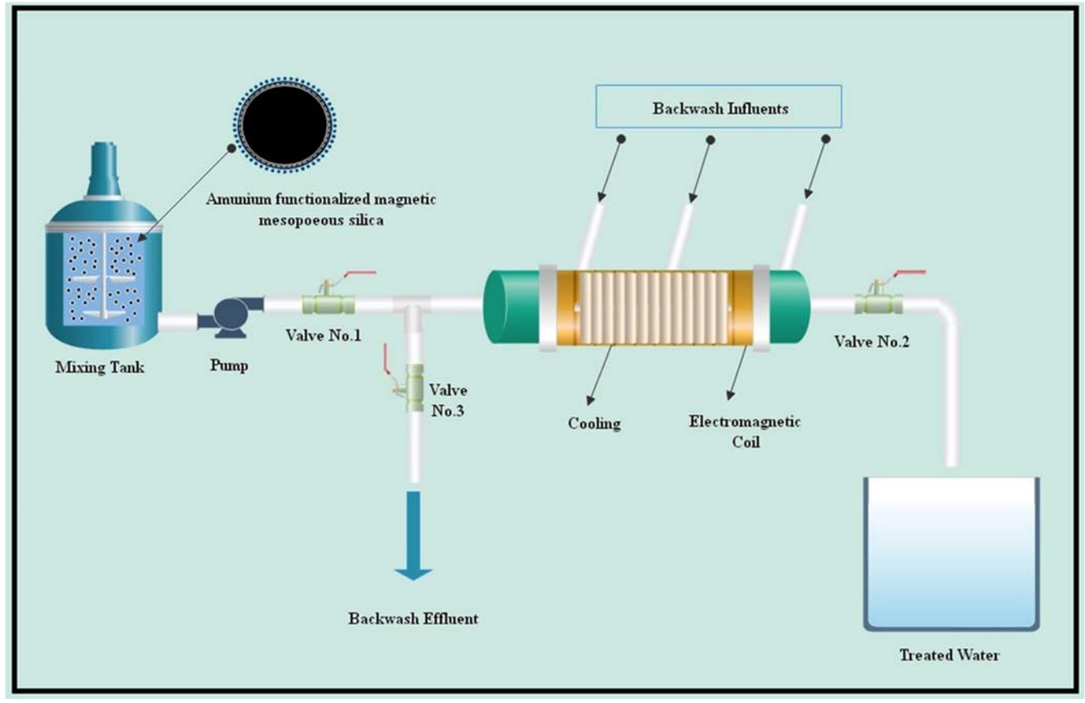

Graphical abstract: Schematic illustration of experimental set-up

Abstract

This paper investigates the adsorption of nitrate anions from aqueous solutions on ammonium-functionalized magnetic mesoporous silica. The adsorbent was prepared via two-step coating process of silica on magnetic core (Fe_3O_4). The resultant structure was modified by 3-aminopropyl triethoxysilane (APTES), and finally acidified in HCl solution to convert the grafted amino groups to ammonium ones. Field-emission scanning electron microscopy (FE-SEM), X-ray diffraction (XRD), vibration sample magnetometer (VSM), Energy-dispersive X-ray spectroscopy (EDX), Fourier transform infrared spectroscopy (FT-IR), and N_2 adsorption/desorption were used to characterize the obtained samples. Experimental results showed that several factors affected the uptake behavior such as pH, contact time, and initial concentration of nitrate. The amount of

sorbent loading were examined and the adsorbent shows great adsorption capacity for NO_3^- (ca.51.28 mg g^{-1} at 25 °C). The nitrate loaded multifunctional microsphere can be easily regenerated with NaOH solution. The separation of multifunctional magnetic microspheres from solution by novel high gradient magnetic separation (HGMS), using the collection of rods, was also investigated in details. Contrast to other methods based on filter and batch conditions, large volumes of water can be easily handled by the new designed HGMS due to the decreasing pressure drop and retention times. The effect of a set of two different experimental variables, i.e. flowrate and magnetic field strength, were investigated to identify the best working conditions for the separation of adsorbent from treated water. The most efficient backwash system was offered to reuse the magnetic particles, too. The removal efficiency of NO_3^- from solution was around 86.24% by the constructed HGMS under the optimal experimental conditions of 7.5 mL s^{-1} flowrate and: 3.49 mT magnitude of the magnetic field.

Keywords: *Adsorption, Ammonium-functionalized magnetic mesoporous silica, Nitrate removal, Magnetic rods, High gradient magnetic separation.*

1. Introduction:

Nitrate can be considered one of the most serious environmental issues in aquatic environments. Contamination of water by Nitrate stems from agricultural wastewater, landfill leachate and improper disposal of industrial and municipal wastes [1, 2]. High nitrate concentration in drinking water can contribute to various health problems. For instance, infants fed with nitrate polluted water are highly likely to suffer from blue baby syndromes, and if untreated, may cause fatal injuries [3]. To protect human health, an allowable level of nitrate concentration ranging around 50 mg L^{-1} NO_3^- has been introduced by World Health Organization (WHO) [4]. Currently, various

physicochemical and biological process including electrodialysis, nano-filtration, ion-exchange, reverse osmosis, and adsorption have been taken into account for the removal of nitrate from aqueous solutions [5-7]. Amongst them, adsorption method showed a promising results, since it offer economical and straightforward operation, resulting in a less sludge generation and disposal issues [8, 9]. So, numerous adsorbents like activated carbon, fly ash and cement, polymeric ion exchangers, mesoporous materials, functionalized polymers and so on have been proposed for the remediation of water polluted by nitrate anions [10-12]. However, these adsorbents have shown poor selectivity, limited surface area, and insignificant adsorption capacity [Table.1]. To address these issues, magnetic nanoparticles have been proposed due to their unique properties including the ease of separation by a simple magnetic field and capability of surface modification [13, 14]. Because of the lower adsorption capacity and susceptibility of magnetic nanoparticle, the core-shell structure has been used where the inner magnetic core is coated with danced silica as an interlayer. This technique can prevent any negative effect on the magnetic core especially under acidic conditions and mesoporous silica as an outer layer owing to its large surface area, tunable pore size and ease of surface modification [15, 16]. Because core-shell magnetic mesoporous silica shows a little adsorption capacity, the functionalization of mesoporous silica plays a vital role. Specifically, the amino-functionalized materials can work for the removal of heavy-metal cations, such as nickel, cadmium, and lead ions as well as for nitrate anion [17, 18]. Although the feasibility of using magnetic particles for water purification has been approved, the capability of using powerful magnetic fields in water treatment process has raised an important question to the scientists.

The high gradient magnetic separation (HGMS) has been a commonly used term recently to meet this demand [19, 20]. This is a physical method to not only separate magnetic particles from fluid

suspension, but also rapid treatment of wastewater. This approach can be applied in a vast number of fields like cleaning up industrial waste, water and sewage treatment, biotechnological field, and mineral processing industry [17, 21]. In principle, the magnetic field can be created by using permanent magnets or electromagnetic coil. Moreover, a ferromagnetic filer, wool, and steel rods are applied across the column placed inside an electromagnet to strengthen the magnetic field, capturing magnetic particles when passing through it [20, 22]. Although the filter matrix and wool have been highly recommended in separating fine magnetic particles, this approach can cause a high pressure drop due to rapid clogging of the filter matrix. As a result, the filter should be quickly replaced or back flushed by a vast amount of solvent, this hinders utilizing of such system on a large-scale. Adopting a combination of rods specially ordered ones can help to deal with these issues and ensure the efficient separation with low operation cost and maximum lifetime. Furthermore, the captured magnetic particles on the steel rods can be dislodged easily by applying backwashing system when the magnetic field is decreased to zero. The HGMS system with low energy consumption, low environmental impact, high magnetic separation capability, and continuous flow process can be considered as a promising separation unit that can combine with an adsorption process to treat wastewater by using magnetic materials.

To our best knowledge, the removal of nitrate by ammonium functionalized core-shell magnetic mesoporous silica combined with lab-scale HGMS system using the ordered rods has not been taken into account in the literature. Consequently, the main aims of the present study are to (1) synthesize and characterize Fe_3O_4@SiO_2@*meso*-SiO_2–NH_2 followed by acidification in HCl solution to convert the grafted amino groups to ammonium moieties (2) model the isotherm data, (3) provide a conceptual design for the HGMS system equipped with a cooling system,

electromagnetic coil, and backwashing, and finally (4) determine the optimal operating conditions for the prepared system.

Table 1. Comparing the adsorption capacity and specific surface area of Fe_3O_4@SiO_2@meso-SiO_2–NH_3^+ with some other adsorbents reported in the literature

Type of adsorbent	Adsorption capacity (mg g^{-1})	Specific surface area (m^2 gr^{-1})	References
Activated carbon	19.28	-	[23]
Di amino-functionalized Mobil Composite Material No. 41 (MCM-41)	38.58	742	[24]
Tri amino-functionalized Mobil Composite Material No. 41 (MCM-41)	36.81	733	[24]
Ion exchange resin (Purolite A520E)	32.3	-	[25]
Polyethylene glycol/chitosan	50.68	2.679	[26]
Polyvinyl alcohol/chitosan	35.03	1.948	[26]
Zinc chloride treated activated carbon	10.2	212.9	[27]
Fe_3O_4@SiO_2@*meso*-SiO_2–NH_3^+	51.28	761.8	This work

2. Materials and methods

2.1. Chemicals

Ferrous chloride tetrahydrate ($FeCl_2 \cdot 4H_2O$), Ferric chloride hexahydrate ($FeCl_3 \cdot 6H_2O$), tetraethylorthosilane (TEOS), ammonium hydroxide (aqueous ammonia 28%wt), absolute ethanol (EtOH), cetyltrimethylammonium bromide (CTAB), and toluene were supplied from Merck Co., USA. 3-Aminopropyl triethoxysilane (APTES 99%) was purchased from Across Co., Germany, and sodium nitrate (KNO_3) was purchased from Aldrich. All chemical reagents and solvents were directly used as received without further purification.

2.2. Preparation of Fe_3O_4@SiO_2@*meso*-SiO_2 microspheres

Fe_3O_4@SiO_2@*meso*-SiO_2 microsphere was prepared according to the method has been explained in the previous work [28] with some modifications. First, 0.1g as-prepared core-shell magnetic silica nanosphere was added into the solution of 40 mL ethanol, 1.3 mL aqueous ammonia, 0.3 g CTAB, 50 mL H_2O and ultra-sonicated for 1 h. Then, 0.5 mL TEOS was added dropwise and stirred for 11 h at 25 °C. Finally, the product was collected, washed with ethanol and deionized water and dried at 60 °C under vacuum overnight. The template was removed by calcination at 560 °C for 5 h under inert gas.

2.3. Preparation of ammonium-functionalized Fe_3O_4@SiO_2@*meso*-SiO_2 microspheres

0.1g of as-prepared Fe_3O_4@SiO_2@*meso*-SiO_2 microspheres were dispersed in 70 mL toluene. Then, 4.5 mL of 3-aminopropyltriethoxysilane (APTES) was added to the solution dropwise. The solution was refluxed at 110 °C for 24 h followed by washing with ethanol and acetone and finally dried under vacuum at 60 °C. After that, the obtained sample was acidified by stirring 50 mg of as-prepared material in 500 mL of 0.1 M HCl for 7 h at 25 °C. The obtained material (Fe_3O_4@SiO_2@*meso*-SiO_2-NH_3^+) was then separated and dried under vacuum for 12 h.

2.4. Material Characterization

The X-ray diffraction (XRD) analysis was obtained on a Bruker AXS D8-advance X-ray diffractometer with CuKα radiation. The Fourier transform infrared (FT-IR) spectra were obtained on a Perkin Elmer FTIR spectrophotometer (USA) with a resolution of 4 cm^{-1}. The size and morphology of the particles were inspected using a field emission scanning electron microscope

(FESEM, Hitachi 1460, Japan). Nitrogen adsorption-desorption isotherms were measured on a PHS-1020 (PHS, China) analyzer at 77 K. The Brunauer–Emmett–Teller (BET) specific surface area was calculated using the adsorption data. Pore size distributions and pore volume were determined by Barret–Joyner–Halenda (BJH) method. The magnetization measurement was performed using a vibration sample magnetometer (VSM; Kavir Magnet Company, Iran). High Precision Balances (Contech Instruments Ltd Co., 0.00001g to 300 g) was used to weigh the amount of Fe_3O_4@SiO_2@*meso*-SiO_2–NH_2 microsphere passed throughout HGMS. The concentrations of nitrate ions in the solution were determined by UV spectrophotometer.

2.5. Adsorption experiments

Adsorption studies of the synthesized adsorbent toward nitrate anion were performed under the following conditions: pH 2-10, adsorbent dosage: 50-400 mg; kinetic time: 10-60 min; and initial concentration: 100-700 mg L^{-1}. Removal of nitrate by adsorbent was investigated in batch experiments. A known amount of particle was stirred for adequate time and then the adsorbent was separated by the magnet from the solution. The supernatant was also analyzed by UV spectrophotometer to obtain the concentration of nitrate anions in the remaining solution. The percent removal of nitrate ions by adsorbent can be expressed by the following expression:

$$R(\%) = \frac{C_i - C_t}{C_i} \times 100 \quad (1)$$

where R is the removal efficiency of nitrate, C_i is the initial concentration and C_t is the concentration of the nitrate ions at time t (mg L^{-1}), respectively.

The equilibrium sorption capacity of the prepared composite can be presented as follows:

$$q_e = C_i - C_e \times \frac{V}{m} \quad (2)$$

where q_e is the equilibrium sorption capacity (mg g^{-1}), C_i and C_e are the initial and equilibrium concentrations of nitrate ion solution, V is the volume of solution, and M is the quantity of the adsorbent (g).

To interpretation of adsorption data, the Langmuir and Freundlich adsorption isotherm models were taken into consideration.

The Langmuir model assumes that each site can only accumulate by one species. The linear form of the Langmuir isotherm can be represented as [29, 30]:

$$\frac{C_e}{q_e} = \frac{1}{K_L q_m} + \frac{C_e}{q_m} \quad (3)$$

where q_e (mg g^{-1}) is the amount adsorbed, q_m (mg g^{-1}) is maximum adsorption capacity, C_e (mg L^{-1}) is the adsorbate concentration and K_L (L mg^{-1}) is the Langmuir constant.

The Freundlich equation is often used to multi-layer sorption and its linearized form is [31, 32]:

$$\ln q_e = \ln K_F + \frac{1}{n} \ln C_e \quad (4)$$

where n and K_F (mg/g) are constants for Freundlich isotherm indicative of the adsorption intensity and adsorption capacity, respectively.

The regeneration of the Fe_3O_4@SiO_2@*meso*-SiO_2@NH_3^+ microsphere was investigated by desorption of nitrate anions from the adsorbent. Commonly, the nitrate loaded sample (250 mg) which is contacted with nitrate solution (300 mg L^{-1}) for 30 min, shaken in a 0.01 mol L^{-1} NaOH for 20 min by ultrasonic, washed with deionized water and acidified in HCl solution to activate positive charges in surface. Finally, the regenerated adsorbent has been dried and added to nitrate solution. These steps represent the first adsorption-desorption cycle, which need to be followed by four other cycles using the same procedure.

2.6. Analysis of HGMS

The efficiency (E) of the backwash system can be calculated via Eq. (5):

$$E(\%) = \frac{M_0 - M_e}{M_0} \times 100 \quad (5)$$

where M_0 and M_e represent the initial magnetite mass in solution (mg) and the mass of magnetite in the effluent obtained from backwash system (mg), respectively.

The separation efficiency of HGMS (E) is defined as follows:

$$E(\%) = \frac{M_0 - M_S}{M_o} \times 100 \quad (6)$$

Where, M_0 (mg) is the mass of adsorbent in the feed solution and M_S (mg) is the mass of adsorbent in the sample passed thought the separation system.

The sample obtained from the outlet of separation was carefully collected by a powerful magnet, then dried under vacuum at 50 °C and weighted with high precision Balances to evaluate the separation efficiency.

2.7. Experimental setup: superconducting magnetic separation

The schematic of the experimental setup is depicted in Fig.1. A laboratory prototype consists of a separation column made of Plexiglas (length and the outer diameter of 290 mm and 21 mm). As it is illustrated in Fig.2 a collection of rods with a diameter of 1.65 mm and a total length of 280 mm in the direction of the flow and perpendicular to the electromagnet coil has also been applied.

A water pump 12 V has been used to pump water to the column in order to remove the captured magnetic particles. There are six valves to control the volume flow rate and backwashing system. During the separation process, the valves No 1, 2 have been opened to guide suspension throughout the separation column while the other valves were closed. In the backwash process, the backwashing water flowed through the separation column with the help of water pump and valves responsible for backwashing. During the backwashing, the electromagnet coil should be turned off

The back wash system is composed of three water jets located in the upper side of column and in the distance of 111 mm, 170 mm and 277 mm from the inlet of flow. To obtain an optimized backwashing system, at first, the performance of one jet situated in the distance of 277 mm from the inlet of flow was examined. Secondly, the backwash system via two water jets, by adding a second jet situated at the distance of 170 mm from the outlet column was taken into consideration. Thirdly, a system with three jets has been taken into account; this system was similar to the

previous system, but with an extra jet at a distance of 111 mm from the outlet. The efficiency of backwash system can be calculated using Equation 5.

The magnet coils (length and the outer diameter of 250 mm and 23 mm) requires continuous cooling during operation since the temperature of coils increase gradually. The cooling station for this system has closed loop with distilled water being circulated through the coils. The return hot water passes through the container equipped with three fans, cooled and pumped back through the coils.

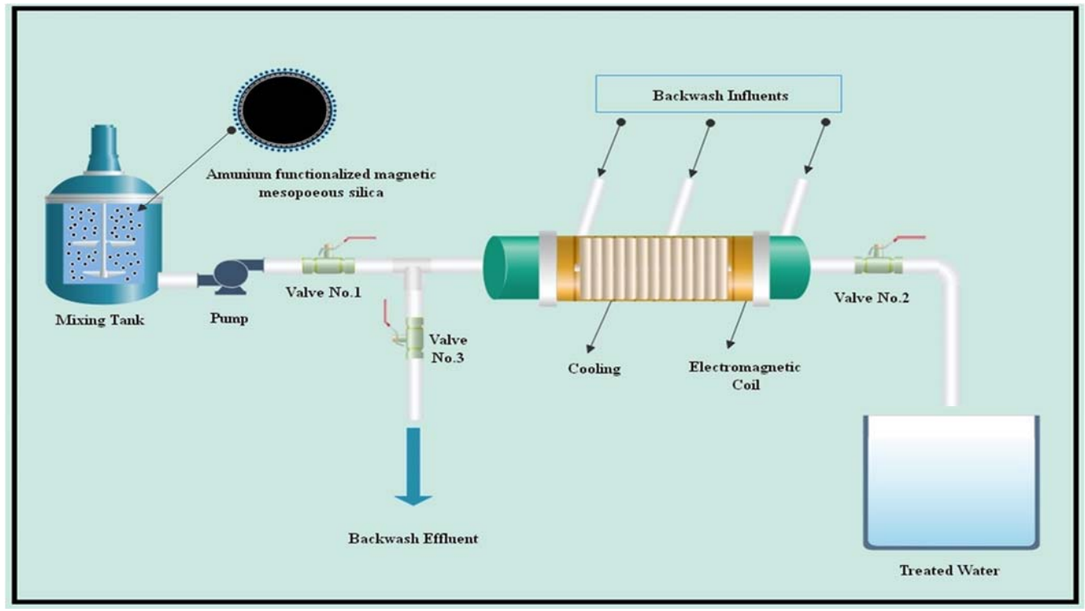

Figure 1. Schematic illusration of the experimental set-up

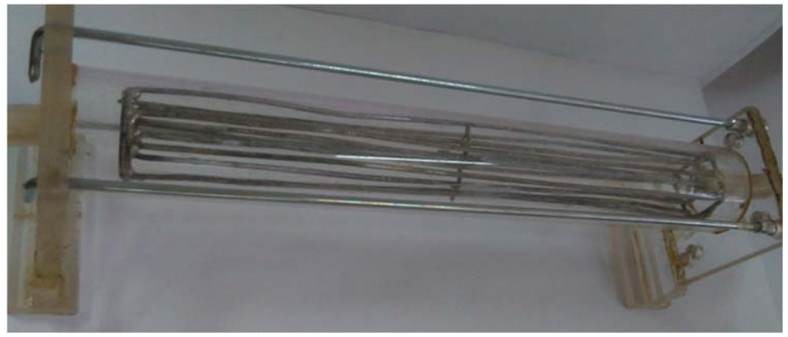

Figure 2. Image the appearance of the filter housing

To optimize the separation condition, the magnitude of the magnetic field in HGMS system was adjusted to be 1.2, 2.37, 3.49, 4.34 mT and the flow rate has been fixed to be 1.6, 4.5, 7.5, 11.3, 15 and 22.5 mL s^{-1}. The effluent of the HGMS system was analyzed and the separation efficiency was calculated according to Equation.6.

All experiments were conducted at ~25°C. Briefly, 5.00 g Fe_3O_4@ SiO_2@*meso*-SiO_2–NH_3^+ microsphere was dispersed in 1.00 L aqueous solution under mechanical stirring (150 rpm). After 15 min, the suspension was continuously flowing through the HGMS system. When the suspension passed through the magnetic separation column, Fe_3O_4@ SiO_2@*meso*-SiO_2–NH_3^+ particles are trapped by the rods situated in the separation column.

It should also be mentioned that each experiment has been repeated 3 times and the small deviations resulted from the inaccuracy of the measurement method could be neglected.

3. Results and discussion

3.1. Characterization of adsorbent

Fig.3 (a) gives the FT-IR spectrums of the ammonium-functionalized magnetic mesoporous silica. The band at 455 cm^{-1} was due to the stretching vibration of the Fe-O bond [33]. The weak and broadband around 3409 cm^{-1} was related to the O-H group resulted from the adsorbed water molecule [34]. Peaks located at 1064 and 786 cm^{-1} corresponded to the antisymmetric and symmetric stretching vibration of Si-O-Si stretching of the silica and mesoporous silica shell, respectively [35, 36]. Moreover, the characteristic vibration bands at 1627 and 1491 cm^{-1} indicating $–NH_3^+$ bending which is originated from amine groups verifying the ammonium functionalization has been successfully achieved [37, 38].

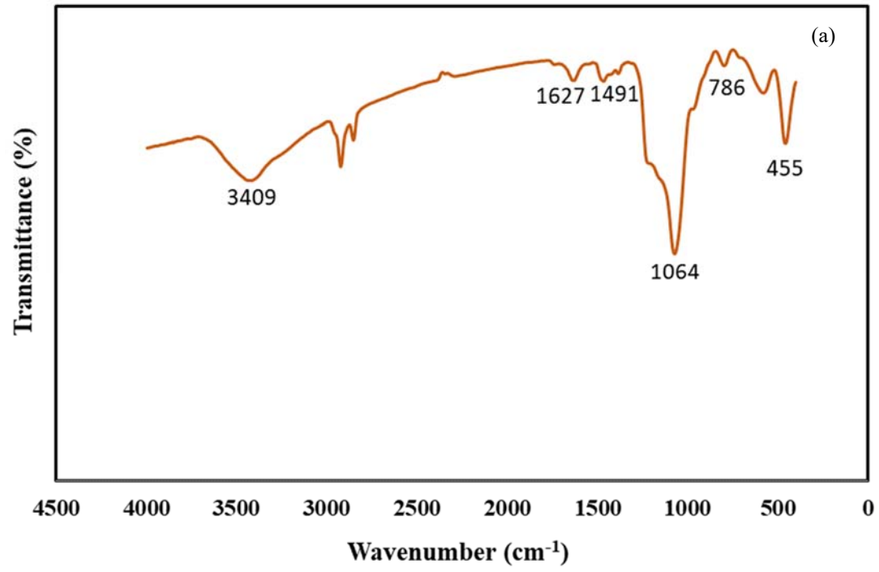

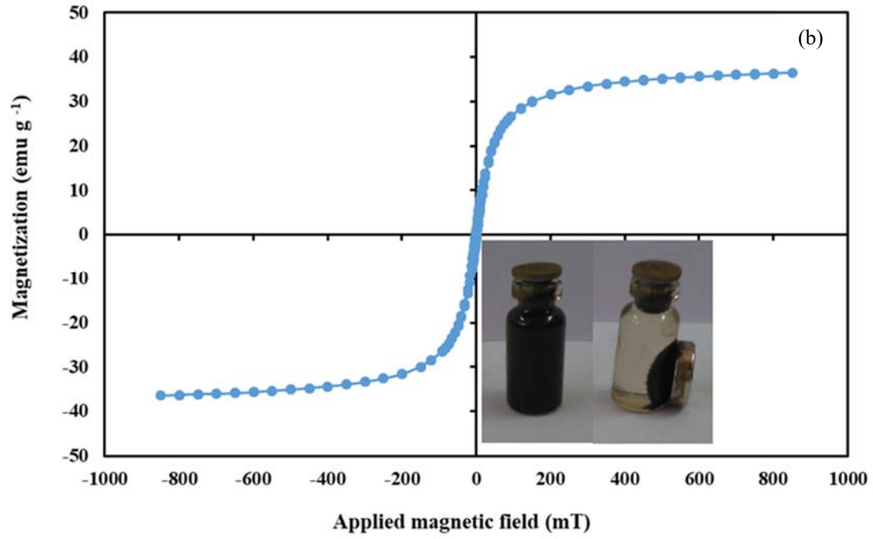
(b)
Magnetization (emu g -1)
50
40
30
20
10
0
-10
-20
-30
-40
-50
-1000
-800
-600
-400
-200
0
200
400
600
800
1000
Applied magnetic field (mT)

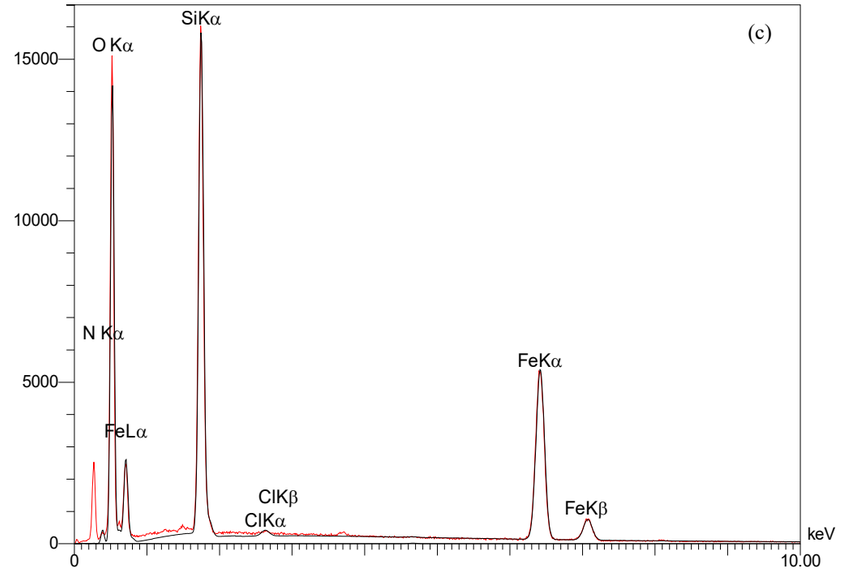
(c)
SiKα
O Kα
N Kα
FeLα
ClKβ
ClKα
FeKα
FeKβ
15000
10000
5000
0
keV
0
10.00

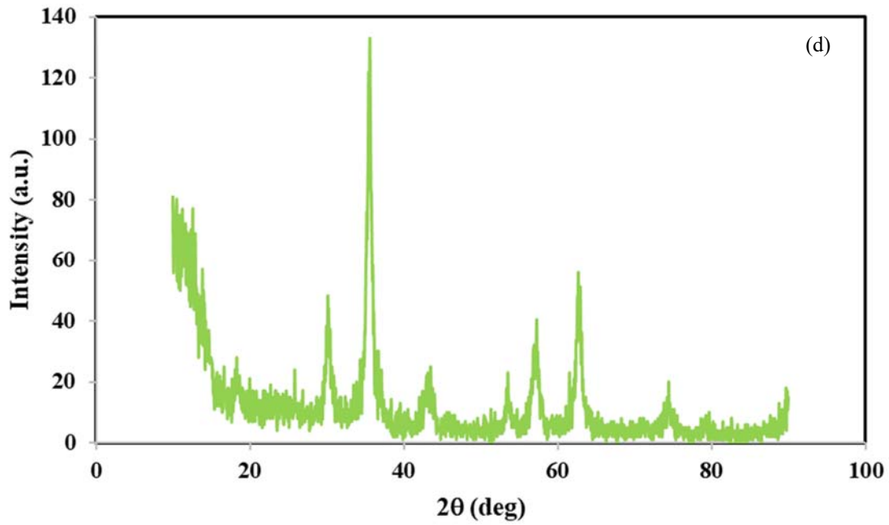

Figure 3. Characterization of Fe_3O_4@ SiO_2@*meso*-SiO_2– NH_3^+ microsphere (a) Fourier transform infrared (FTIR) spectra, (b) magnetization curve (The inset is the magnetic separation of adsorbent from suspension), (c) EDX spectrum at 10 kV acceleration voltage, and (d) Powder X-ray diffraction (XRD) pattern,

The hysteresis loops and magnetic properties of Fe_3O_4@SiO_2@*meso*-SiO_2@ NH_3^+ was assessed by VSM. As presented in Fig.3 (b), the magnetic saturation of Fe_3O_4@SiO_2@*meso*-SiO_2@ NH_3^+ was 36.45 emu g^{-1}. Moreover, no remanence for the obtained sample confirms the superparamagnetic features. As a result, this particle can be separated from the aqueous solution in less than 60 s (Fig.3 (b), insert). The achieved result shows that the unique strategy to remove surfactant is highly beneficial to obtain a magnetic material with high magnetization value, which provides the prompt separation of particle with minimum required energy by HGMS.

The atomic and weight percentages of the elements in Fe_3O_4@SiO_2@*meso*-SiO_2@ NH_3^+ were examined by EDX analysis. As it is illustrated in Fig. 3(c), C, Si, N, Fe, and O were all exist in the prepared adsorbent [39]. Quantitative results of EDX analysis are shown in Table.2.

The crystalline structures of the Fe_3O_4 and Fe_3O_4@SiO_2@*meso*-SiO_2@NH_3^+ were identified with XRD. As presented in Fig.3(d) five characteristic diffraction peaks with 2θ at 30.2º, 35.6º, 43.3º, 53.8º, 57.3º, and 63.0º were observed, reflections of inverse spinel Fe_3O_4 and reflected that there was no crystal transition of the magnetic nanoparticles during the coating and grafting process [40]. Meanwhile, the broad peak centered around 2θ=24º assigned to amorphous silica of silica layer.

Table 2. Quantitative Results of EDX analysis.

Elt	Line	Int	K	Kr	W%	A%	ZAF	Ox%	Pk/Bg	Class	LConf
N	Ka	19.0	0.0306	0.0171	5.22	7.91	0.3270	0.00	62.05	A	4.98
O	Ka	716.4	0.3931	0.2192	52.97	70.23	0.4139	0.00	541.28	A	52.57
Si	Ka	1138.2	0.1785	0.0995	15.73	11.88	0.6328	0.00	46.64	A	15.64
Cl	Ka	21.7	0.0045	0.0025	0.33	0.20	0.7537	0.00	2.72	B	0.32
Fe	Ka	799.5	0.3933	0.2193	25.76	9.78	0.8516	0.00	40.58	A	25.57
			1.0000	0.5577	100.00	100.00		0.00			

The morphological and structural features of the samples were determined by FE-SEM. As shown in Fig.4, the Fe_3O_4, Fe_3O_4@SiO_2, and Fe_3O_4@SiO_2@*meso*-SiO_2@ NH_3 exhibit monodispersed spherical morphology and narrow size distribution. Their mean particle sizes were also measured to be 10, 15 and 320 nm, respectively.

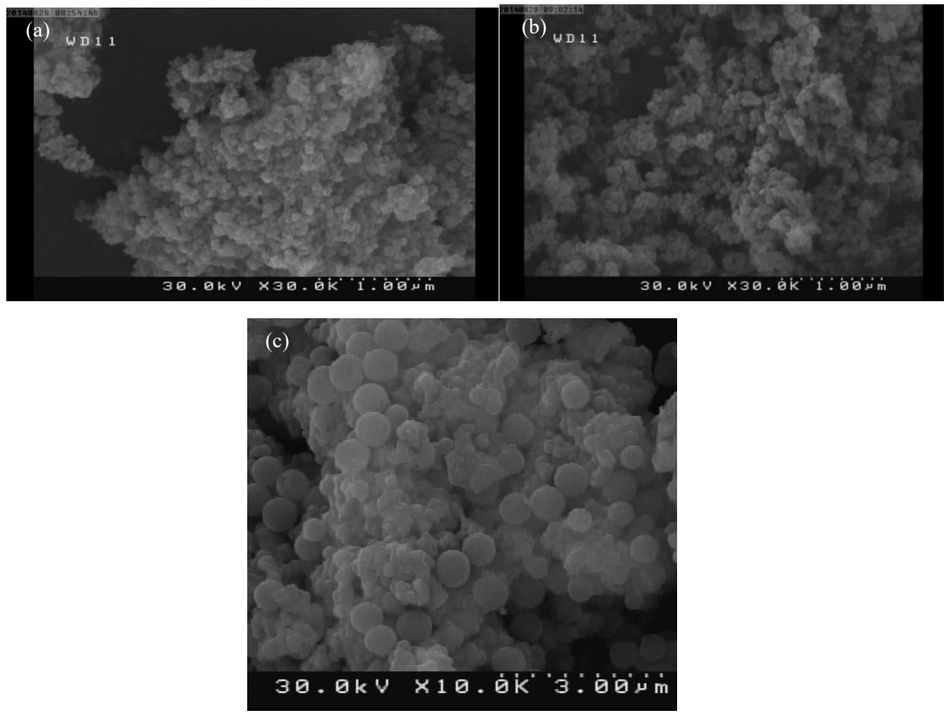

Figure 4. Field emission scanning electron microscope (FESEM) images of (a) Fe_3O_4, (b) Fe_3O_4@SiO_2, and (c) Fe_3O_4@SiO_2@*meso*-SiO_2@ NH_3^+ microsphere.

The N_2 adsorption/desorption isotherms of Fe_3O_4@SiO_2@*meso*-SiO_2 and Fe_3O_4@SiO_2@*meso*-SiO_2@NH_3^+ were used to assess the surface properties of synthesized particles. As shown in Fig.5, two samples exhibit typical IV-typed isotherms with H3-hysteresis loops, associating with mesoporous material according to IUPAC classification [41]. The BET surface area of Fe_3O_4@SiO_2@*meso*-SiO_2 microsphere were reported to be 878.58 m^2 g^{-1}. After ammonium-functionalization, BET surface area of Fe_3O_4@SiO_2@*meso*-SiO_2@NH_3^+ microsphere decreases to 761.5 m^2 g^{-1}.

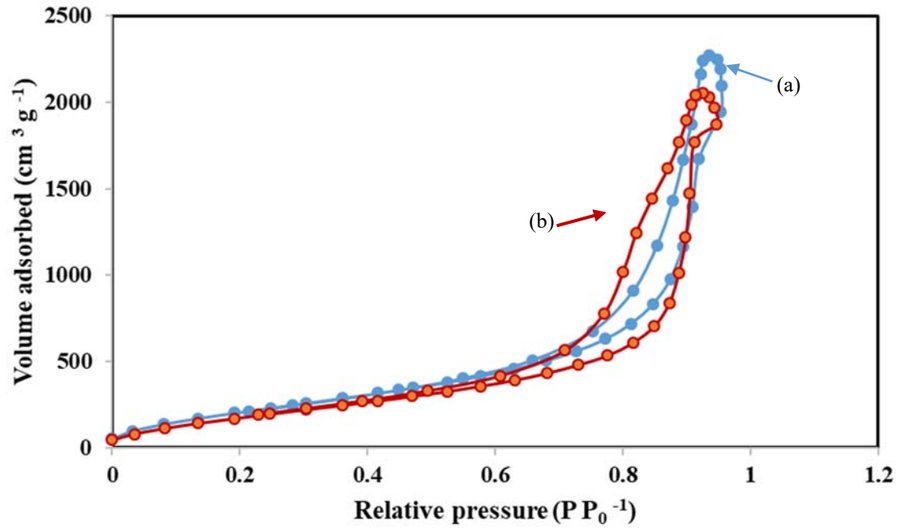

Figure 5. Nitrogen adsorption–desorption isotherms of (a) Fe_3O_4@SiO_2@*meso*-SiO_2, and (b) Fe_3O_4@SiO_2@*meso*-SiO_2@ NH_3^+ microsphere.

3.2. Nitrate removal studies

3.2.1. Effect of pH and kinetic time

The pH of the solution is one of the most important factors on adsorbent surface charge and the adsorption of nitrate anions. As presented in Fig.6 (a) within the pH range 2 to10, the removal efficiency was not affected by the pH and that was attributed to the competition of the vast amount of Cl^- with the nitrate ion exchange. In contrast, at pH > 8, the removal efficiency was negatively affected by the pH. This stems from the deprotonation of the propyl-amine groups grafted on the mesoporous silica. As a result, the negative sites of adsorbent hindered the adsorption of NO_3^-. Moreover, the pK_a value for amino-functionalized mesoporous silica structures was calculated to be ~9 [42, 43]. Therefore, when pH < pK_a, the propyl amino groups became positively charged due to their protonation, which results in attracting nitrate anions by ammonium moieties via

electrostatic forces [Fig.6 (b)]. On the other hand, when pH > p*K*a, the modified amino groups were deprotonated, which disabled them to employ any electrostatic force toward NO_3^-. Therefore, the maximum removal efficiency of nitrate ion was obtained at pH 6.

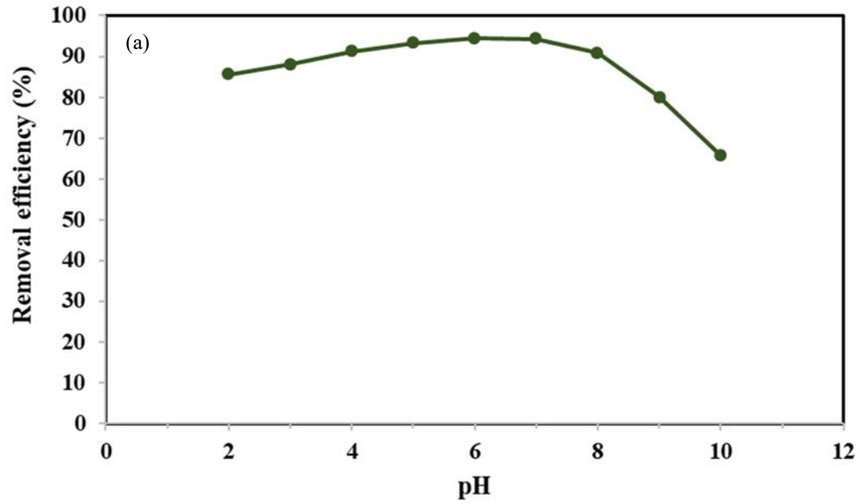

(b)

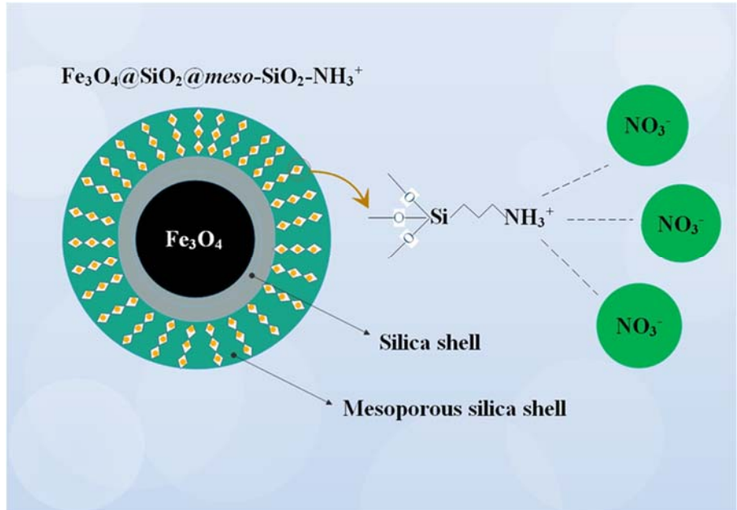

Figure 6. (a) Effect of pH on the adsorption of NO_3^-; adsorbent: 250 mg, initial concentration of nitrate anions: 300 mg L^{-1}, volume of NO_3^- solution: 50 mL, contact time: 60 min, at 298 K, (b) Adsorption mechanism of nitrate onto the Fe_3O_4@SiO_2@meso-SiO_2–NH_3^+

3.2.2. Effect of kinetic time and sorbent dosage

The effect of kinetic time on the removal of NO_3^- was examined when the initial nitrate anion was selected as 300 mg L^{-1}. As illustrated in Fig.7 (a) a great amount of nitrate anions has been removed within the first 10 min that stem from the grafting of higher content of the ammonium group into the mesoporous structure and many active sites to adsorb nitrate ions. The maximum removal efficiency has been attained within 30 min and then it kept almost unchanged for the remained time. To guarantee the complete removal, a contact period of 60 min was selected for further experiments.

The effect of adsorbent loading on the removal efficiency of nitrate ions is shown in Fig.7 (b). Various amount (50–400 mg) of as-prepared material were added to nitrate solutions and removal efficiency was calculated for each solution. It is clear that the nitrate removal increases with rising the amount of adsorbent loading from 50 to 250 mg. This is maybe due to the availability of more adsorption sites at higher sorbent dosage. However, at an extra adsorbent loading (over 250 mg) only a fraction of available binding sites on the adsorbent surface is occupied by nitrate ions due to a vast number of those binding sites. Therefore, the removal efficiency did not improve significantly as a result of low equilibrium adsorbent nitrate concentration.

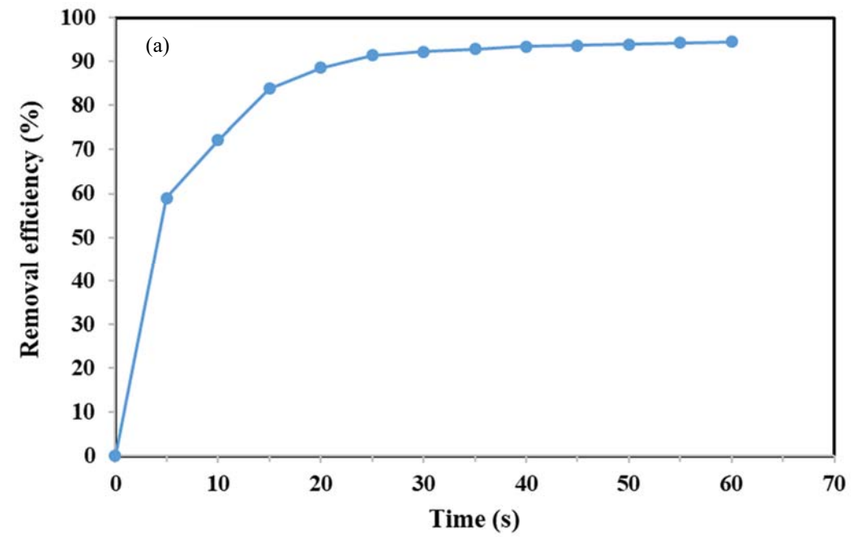

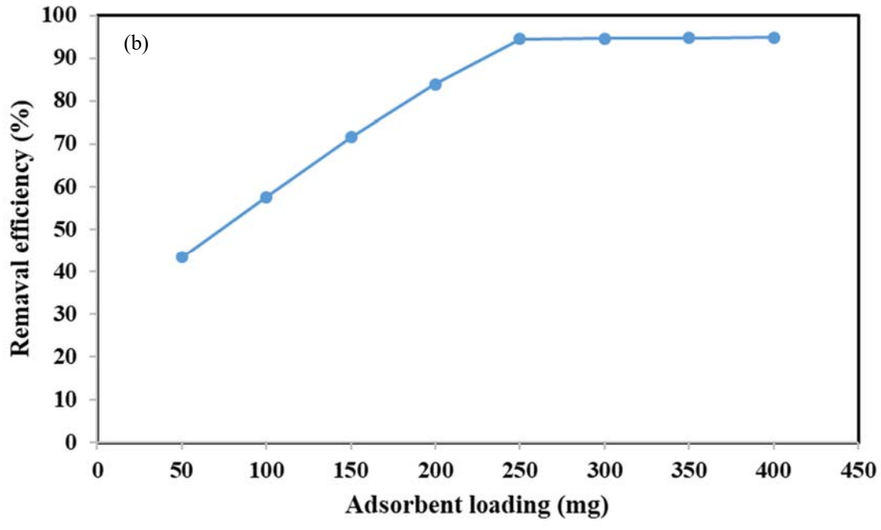

Figure 7. Effect of (a) time on the adsorption of NO_3^-, and (b) sorbent dosage on adsorption. (Optimum conditions for both experiments: Initial concentration of nitrate anions: 300 mg L^{-1}, volume of NO_3^- solution: 50 mL, pH: 6, at 298 K).

3.2.3. Adsorption isotherms

The equilibrium adsorption studies of Fe_3O_4@SiO_2@*meso*-SiO_2@NH_3^+ microsphere need to be conducted in a different initial concentrations of nitrate ion (100 to 700 mg L^{-1}). After that, two adsorption models named Langmuir and Freundlich (Eqs. (3) and (4)) have been examined to find the one that is in good agreement with our results and expresses how the adsorption process is controlled. The adsorption isotherm of NO_3^- on the adsorbent is displayed in Fig.8 (a). The adsorption capacity of adsorbents for nitrate anions rapidly increased with rising initial concentration and then gradually become constant until reaching equilibrium.

The fitted experimental data with both models are depicted in Fig.8 (b), (c). The fitting parameters achieved from the curve-fitting results are shown in Table.3. The results indicate that the experimental data are fitted well w Langmuir model, correlation coefficient (0.98). These results confirm that the constant energy of adsorption and monolayer adsorption of the nitrate ion onto the adsorbent. The maximum adsorption value calculated by the Langmuir equation is 51.28 mg g^{-1}

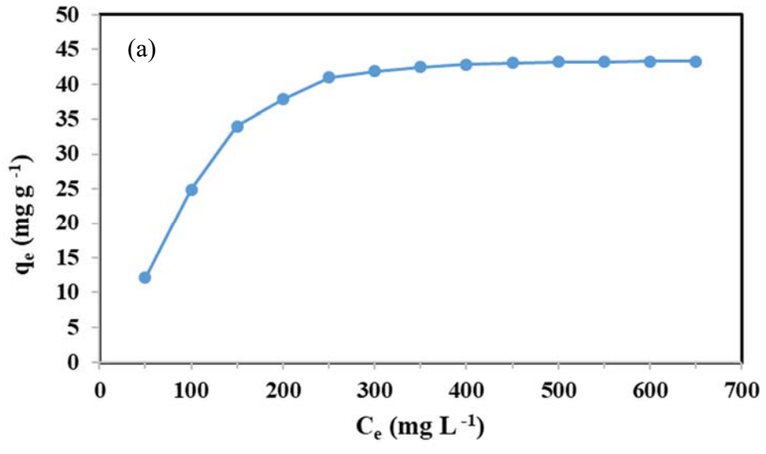

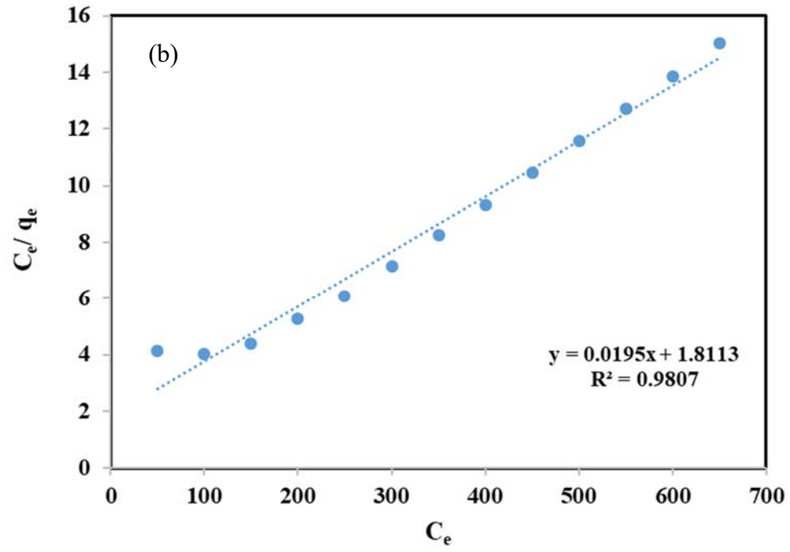

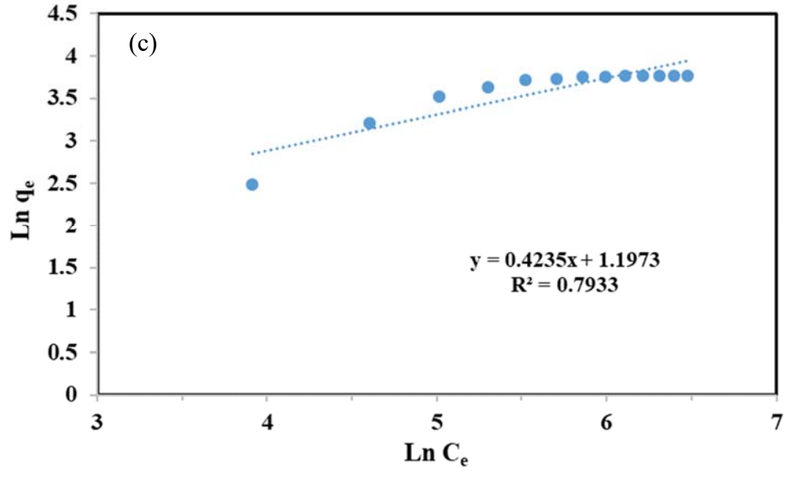

Figure 8. Equilibrium adsorption isotherm (a) of NO_3^- by Fe_3O_4@SiO_2@*meso*-SiO_2@ NH_3^+ microsphere, Langmuir (b) and Freundlich (c) isotherms of nitrate adsorption. Adsorbent: 250 mg, volume of NO_3^- solution: 50 mL, pH: 6, contact time: 60 min, at 298 K.

Table 3.Calculated values of parameters in Langmuir and Freundlich equation.

Langmuir equation			Freundlich equation		
q_m (mg g^{-1})	k_L (L mg^{-1})	R^2	k_f (mg g^{-1}) ((mg L^{-1}) $^{(n)-1}$)$^{-1}$	n	R^2
51.28	0.0108	0.9807	3.311	2.36	0.7933

3.2.4. Reusability of Fe_3O_4@SiO_2@*meso*-SiO_2@ NH_3^+ microsphere

The regeneration of the Fe_3O_4@SiO_2@*meso*-SiO_2@NH_2 microsphere is a crucial because it helps to recover nitrate as valuable fertilizers, reuse the adsorbent, and preserve the environment from solid waste disposal issue. As it is shown in Fig.9, the adsorption capacity of ammonium-functionalized magnetic mesoporous silica remained almost unchanged after 5 cycles. This result suggests that the prepared adsorbent possess excellent reusability.

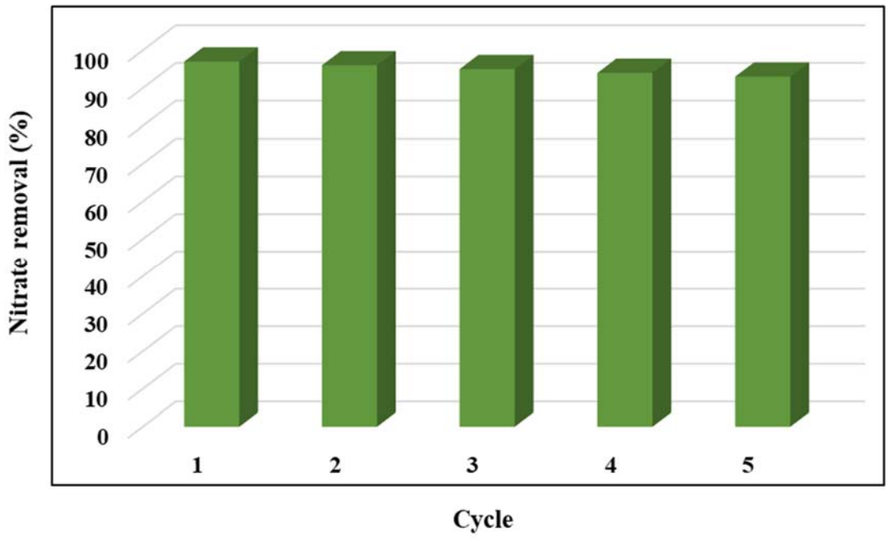

Figure 9. Regeneration studies of Fe_3O_4@SiO_2@*meso*-SiO_2@ NH_3^+ microsphere.

3.3. Fe_3O_4@SiO_2@*meso*-SiO_2@ NH_3^+ microspheres removal by HGMS system

Experiments on the impact of flow rate on separation efficiency were performed at different flow rates: 4.5, 7.5, 11.3, 15 and 22.5 ml s^{-1}, while the magnitude of the magnetic field was kept constant at 3.49 mT. As it can be seen from Fig.10 (a), the maximum capture efficiency for the 1.6, 4.5, 7.5, 11.3, 15 and 22.5 mL s^{-1} was reported to be 89%, 87.54%, 83.19%, 78.68%, and 74.18%, respectively. By increasing the flow rate, HGMS was not able to separate all particles resulting in a decrease in the separation efficiency. This might be attributed to the lower residence time of the magnetic materials in HGMS and increasing hydrodynamic drag acting upon the particles, consequently some of them passed through the separator at higher flow rate. In this respect, 7.5 mL s^{-1} was chosen as the optimum flow rate for the following experiments.

Fig.10 (b) shows the separation efficiency of Fe_3O_4@SiO_2@*meso*-SiO_2@NH_3^+ microspheres at a different magnetic intensity of 1.2, 2.37, 3.49, 4.34 mT, when the flow rate was 7.5 mL s^{-1}. The maximum separation efficiencies for 1.2, 2.37, 3.49, 4.34 mT were obtained to be 79.5%, 84.49%, 87.54%, and 89.32%, respectively. The results revealed that increasing the magnetic field resulted in more magnetic particles to be captured by the HGMS instead of being passed through the device. Although, the highest efficiency has been achieved at the magnetic field of 4.34 mT, the experiments have been performed at 3.49 mT because only about 2% of separated particle increased at the magnetic field of 4.34 mT. Furthermore, the lower value of magnetic field leads to lower energy consumption and lower heat generation, which would drastically reduce the operating costs especially in an industrial-scale.

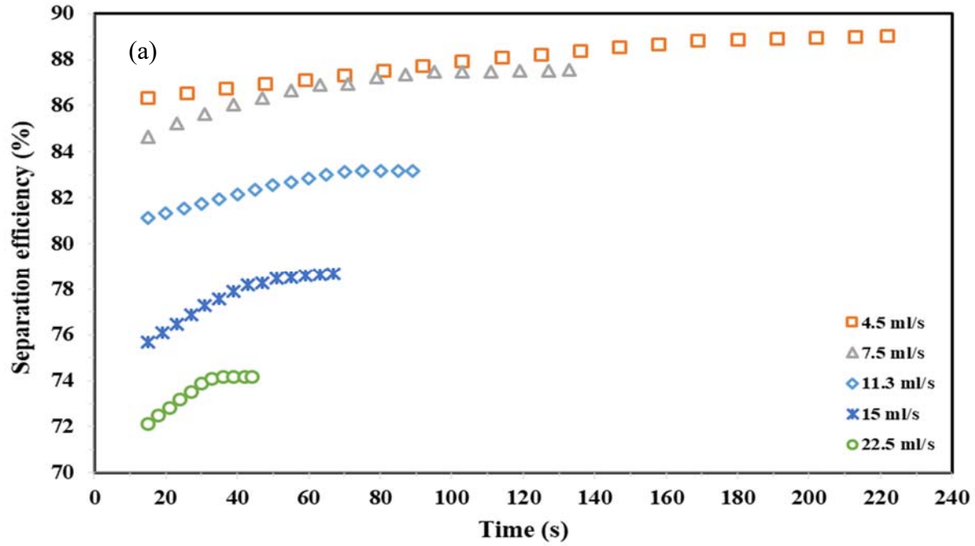

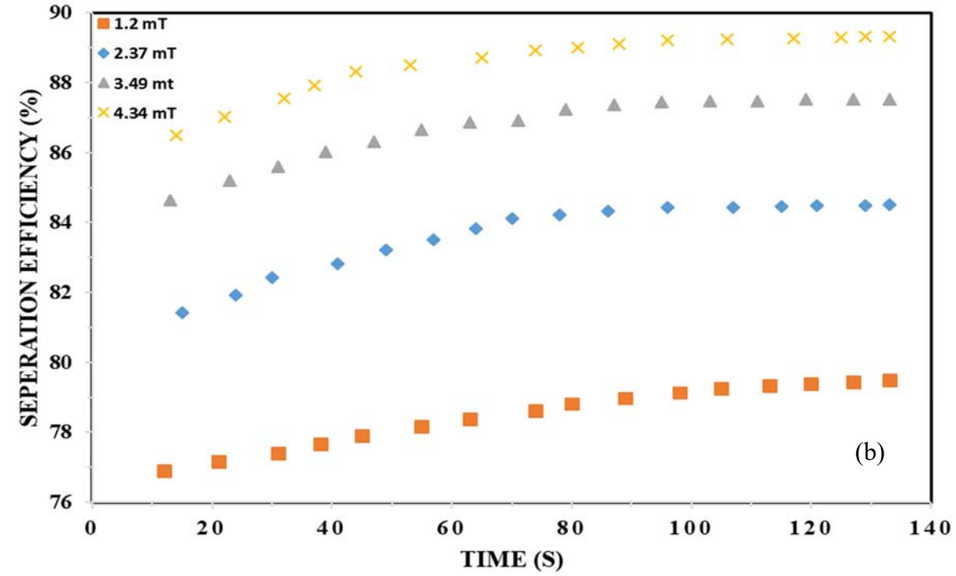

Figure 10. Separation efficiency of Fe3O4@SiO2@meso-SiO2@ NH3+ microsphere at (a) different flowrate. Magnitude of the magnetic field: 3.49 mT, (b) different magnetic field strength. Flow rate: 7.5 mL s−1

As it is represented in Table.4, the efficiency of backwashing has been obtained to be 84.3%, 88.9%, and 95.4% for one jet, two and three jets. Furthermore, the required water and time has been decreased by raising the number of water jet and it has been reported to be (710 mL, 56s), (430 mL, 34s), and (240 mL, 21s) for one jet, two and three jets, respectively. In this regard, the backwashing with 3 water jets is selected as an optimized arrangement for the proposed system from an economic point of view as it not only shows higher efficiency but also needs a minimum amount of water and time.

Table 4.Details of different backwashing systems.

Number of water jet	Required time (s)	Required water (mL)	Efficiency (%)
1	56	710	84.3
2	43	430	88.9
3	21	240	95.4

3.4. Removal of NO^{3-} from solution by HGMS system

The removal efficiency of nitrate from solution has been investigated by the laboratory-scale of the HGMS under the optimal operating conditions, i.e., magnetic field= 3.49 mT, flowrate= 7.5 mL s^{-1}, pH=6, kinetic time= 60 min, initial concentration=300 mg L^{-1}, volume of NO^{3-} solution: 1.00 L, amount of adsorbent=5.00 g (Fig.11). The removal efficiency of nitrate rose considerably from 83.3% to 86.15% within 95 s. This may be attributed to the leakage of adsorbent from the HGMS system because of the available free space in the separation column over the first 95 s.

After 95 s, the free space have been filled up by the trapped particles and prevents adsorbent from leaving the separation. Therefore, the removal efficiency remained almost unchanged. The maximum removal efficiency has been reported to be 86.24% at the end of the process.

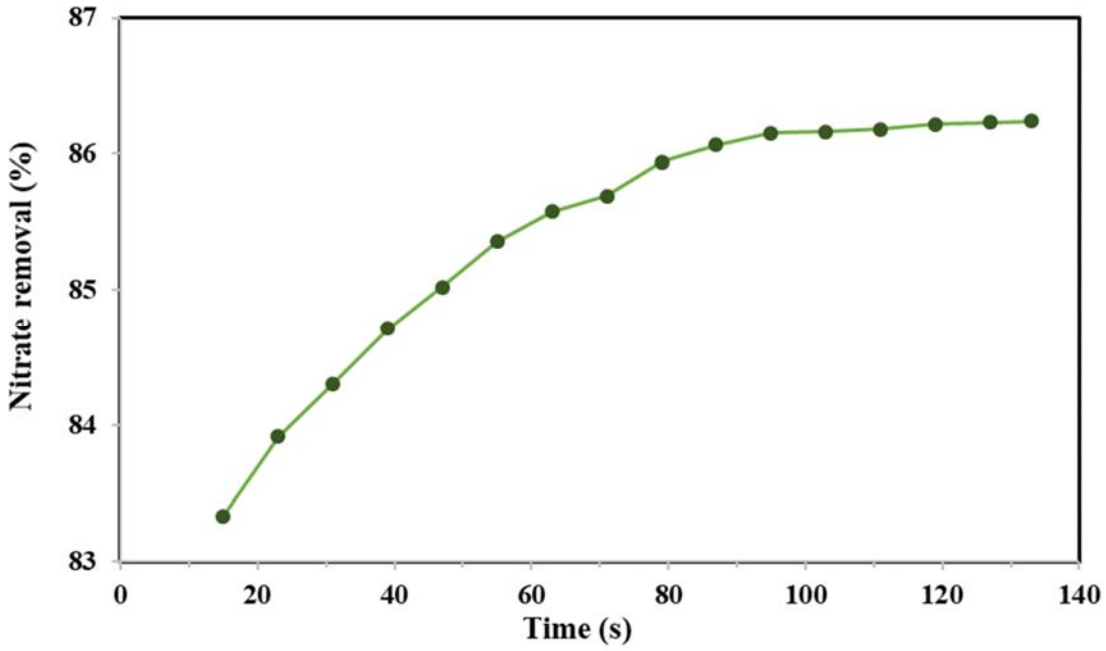

Figure 10. The removal of NO_3^- by HGMS. Flow rate: 7.2 mL s^{-1}, magnetic field: 3.49 mT, pH=6, contact time= 60 min, initial concentration=300 mg L^{-1}, volume of NO_3^- solution: 1.00 L, dose of adsorbent=5.00 g

4. Conclusions

In this study, ammonium-functionalized magnetic mesoporous silica has been successfully synthesized to remove nitrate anions from aqueous solutions. Batch experiments were performed at a different kinetic time, pH, sorbent loading and initial concentration of nitrate. The results showed that the adsorption reached equilibrium within ca. 30 min when pH and sorbent loading

were fixed at 6 and 250 mg, respectively. The equilibrium data were analyzed using the Langmuir and Freundlich isotherm models and it was found that the sorption of nitrate anions was well fitted to the Langmuir equation. The maximum adsorption capacity of adsorbent was also obtained to be 51.28 mg g^{-1} at 25 °C. Effective recovery of nitrate anions was obtained with NaOH solution and adsorbent exhibited a good reusability. The performance of the HGMS system to remove Fe_3O_4@SiO_2@meso-SiO_2@NH^{3+} has been taken into consideration, too. In the operation conditions of a flow rate of 7.5 mL s^{-1} and magnetic field of 3.49 mT, the separation efficiency of 87.54% has been achieved. The backwashing with 3 water jets was also selected as most efficient arrangement for the removal of captured adsorbent by HGMS. The removal efficiency of NO^{3-} from solution has been investigated by the experimental-scale of the HGMS under the optimal operating conditions, and the results indicated that the removal efficiency of nitrate anions went up significantly to a peak of 86.24%.

Acknowledgments

This work was supported by Shiraz University Entrepreneurship Center Grant Number KNM/3081. The authors are immensely thankful to Dr. Gh. Absalan, Professor Masoumi Laboratory, department of chemistry, college of science, Shiraz University, for his helpful advice and devoting his laboratories facilities. The assistance of Dr. S. Javadpour, Materials Science & Engineering department, Shiraz University for the magnetization measurements. We would also like to show our gratitude to Dr. Kh. Jafarpur, School of Mechanical Engineering, Shiraz University, for his valuable comments on the experimental set-up.

References

[1] S. Tyagi, D. Rawtani, N. Khatri, and M. Tharmavaram, Strategies for Nitrate removal from aqueous environment using Nanotechnology: A Review, Journal of Water Process Engineering. 21 (2018) 84-95.

[2] S. Kilpimaa, H. Runtti, T. Kangas, U. Lassi, and T. Kuokkanen, Removal of phosphate and nitrate over a modified carbon residue from biomass gasification, Chemical Engineering Research and Design. 92 (2014) 1923-1933.

[3] A. Bhatnagar and M. Sillanpää, A review of emerging adsorbents for nitrate removal from water, Chemical Engineering Journal. 168 (2011) 493-504.

[4] W. H. Organization, *Guidelines for drinking-water quality: recommendations* vol. 1: World Health Organization, 2004.

[5] J. Markovski, J. Garcia, K. D. Hristovski, and P. Westerhoff, Nano-enabling of strong-base ion-exchange media via a room-temperature aluminum (hydr) oxide synthesis method to simultaneously remove nitrate and fluoride, Science of the Total Environment. 599 (2017) 1848-1855.

[6] F. D. Belkada, O. Kitous, N. Drouiche, S. Aoudj, O. Bouchelaghem, N. Abdi*, et al.*, Electrodialysis for fluoride and nitrate removal from synthesized photovoltaic industry wastewater, Separation and Purification Technology. 204 (2018) 108-115.

[7] N. Ghaemi, P. Daraei, and F. S. Akhlaghi, Polyethersulfone nanofiltration membrane embedded by chitosan nanoparticles: Fabrication, characterization and performance in nitrate removal from water, Carbohydrate polymers. 191 (2018) 142-151.

[8] A. Bhatnagar, E. Kumar, and M. Sillanpää, Fluoride removal from water by adsorption—a review, Chemical Engineering Journal. 171 (2011) 811-840.

[9] M. Ahmadzadeh Tofighy and T. Mohammadi, Nitrate removal from water using functionalized carbon nanotube sheets, Chemical Engineering Research and Design. 90 (2012) 1815-1822.

[10] S. Shukla, V. Gaikar, R. S. Pai, and U. S. Suryavanshi, Batch and column adsorption of Cu (II) on unmodified and oxidized coir, Separation Science and Technology. 44 (2009) 40-62.

[11] L.-C. Zhou, Y.-F. Li, X. Bai, and G.-H. Zhao, Use of microorganisms immobilized on composite polyurethane foam to remove Cu (II) from aqueous solution, Journal of Hazardous Materials. 167 (2009) 1106-1113.

[12] H. I. Uzun and E. Debik, Economical approach to nitrate removal via membrane capacitive deionization, Separation and Purification Technology. 209 (2019) 776-781.

[13] C. Meng, W. Zhikun, L. Qiang, L. Chunling, S. Shuangqing, and H. Songqing, Preparation of amino-functionalized Fe3O4@ mSiO2 core-shell magnetic nanoparticles and their application for aqueous Fe3+ removal, Journal of hazardous materials. 341 (2018) 198-206.

[14] X. Chen, B. Zhang, Y. Liu, C. Zhao, H. Zhang, and Q. Zhang, Effect of embedded sodium polyacrylate chains on the adsorption mechanism of neutral red by magnetic particles, Chemical Engineering Research and Design. 127 (2017) 223-235.

[15] M. Xuan, J. Shao, J. Zhao, Q. Li, L. Dai, and J. Li, Cover Picture: Magnetic Mesoporous Silica Nanoparticles Cloaked by Red Blood Cell Membranes: Applications in Cancer Therapy (Angew. Chem. Int. Ed. 21/2018), Angewandte Chemie International Edition. 57 (2018) 5955-5955.

[16] L. Wan, H. Song, X. Chen, Y. Zhang, Q. Yue, P. Pan*, et al.*, A Magnetic□Field Guided Interface Coassembly Approach to Magnetic Mesoporous Silica Nanochains for Osteoclast□Targeted Inhibition and Heterogeneous Nanocatalysis, Advanced Materials. 30 (2018) p 1707515.

[17] H. Zheng, D. Hu, L. Zhang, and T. Rufford, Thiol functionalized mesoporous silicas for selective adsorption of precious metals, Minerals Engineering. 35 (2012) 20-26.

[18] G. Z. Kyzas, E. A. Deliyanni, D. N. Bikiaris, and A. C. Mitropoulos, Graphene composites as dye adsorbents: Review, Chemical Engineering Research and Design. 129 (2018) 75-88.

[19] Z. Qi, T. P. Joshi, R. Liu, Y. Li, H. Liu, and J. Qu, Adsorption combined with superconducting high gradient magnetic separation technique used for removal of arsenic and antimony, Journal of hazardous materials. 343 (2018) 36-48.
[20] Q. Wang, Y. Guan, X. Ren, M. Yang, and X. Liu, Removal of low concentration Cr (VI) from aqueous solution by magnetic-fluids fixed bed using the high gradient magnetic separation, Journal of colloid and interface science. 374 (2012) 325-330.
[21] G. Altın, S. İnal, and A. İbrahim, Recovery of chromite from processing plant Tailing by vertical ring and pulsating High-Gradient magnetic separation, MT Bilimsel. 13 (2016) 23-35.
[22] F. Mishima, S. Takeda, M. Fukushima, and S. Nishijima, A superconducting magnetic separation system of ferromagnetic fine particles from a viscous fluid, Physica C: Superconductivity and its applications. 463 (2007) 1302-1305.
[23] S. Jiang, H. Wang, G. Xiong, X. Wang, and S. Tan, Removal of nitrate using activated carbon-based electrodes for capacitive deionization, Water Science and Technology: Water Supply. 18 (2018) 2028-2034.
[24] M. Ebrahimi-Gatkash, H. Younesi, A. Shahbazi, and A. Heidari, Amino-functionalized mesoporous MCM-41 silica as an efficient adsorbent for water treatment: batch and fixed-bed column adsorption of the nitrate anion, Applied Water Science. 7 (2017) 1887-1901.
[25] T. Nur, W. Shim, P. Loganathan, S. Vigneswaran, and J. Kandasamy, Nitrate removal using Purolite A520E ion exchange resin: batch and fixed-bed column adsorption modelling, International journal of environmental science and technology. 12 (2015) 1311-1320.
[26] A. Rajeswari, A. Amalraj, and A. Pius, Adsorption studies for the removal of nitrate using chitosan/PEG and chitosan/PVA polymer composites, Journal of Water Process Engineering. 9 (2016) 123-134.
[27] R. Kamaraj and S. Vasudevan, Decontamination of selenate from aqueous solution by oxidized multi-walled carbon nanotubes, Powder Technology. 274 (2015) 268-275.
[28] Z. Kheshti and S. Hassanajili, Novel Multifunctional Mesoporous Microsphere with High Surface Area for Removal of Zinc Ion from Aqueous Solution: Preparation and Characterization, Journal of Inorganic and Organometallic Polymers and Materials. 27 (2017) 1613-1626.
[29] F. Ge, M.-M. Li, H. Ye, and B.-X. Zhao, Effective removal of heavy metal ions Cd2+, Zn2+, Pb2+, Cu2+ from aqueous solution by polymer-modified magnetic nanoparticles, Journal of hazardous materials. 211 (2012) 366-372.
[30] Y. Zhu, J. Hu, and J. Wang, Competitive adsorption of Pb (II), Cu (II) and Zn (II) onto xanthate-modified magnetic chitosan, Journal of hazardous materials. 221 (2012) 155-161.
[31] L. Jiang, S. Li, H. Yu, Z. Zou, X. Hou, F. Shen, *et al.*, Amino and thiol modified magnetic multi-walled carbon nanotubes for the simultaneous removal of lead, zinc, and phenol from aqueous solutions, Applied Surface Science. 369 (2016) 398-413.
[32] S. Lapwanit, T. Trakulsujaritchok, and P. N. Nongkhai, Chelating magnetic copolymer composite modified by click reaction for removal of heavy metal ions from aqueous solution, Chemical Engineering Journal. 289 (2016) 286-295.
[33] Z. Xu, Y. Feng, X. Liu, M. Guan, C. Zhao, and H. Zhang, Synthesis and characterization of Fe3O4@ SiO2@ poly-l-alanine, peptide brush–magnetic microspheres through NCA chemistry for drug delivery and enrichment of BSA, Colloids and Surfaces B: Biointerfaces. 81 (2010) 503-507.
[34] P. Xu, H. Wang, R. Tong, Q. Du, and W. Zhong, Preparation and morphology of SiO 2/PMMA nanohybrids by microemulsion polymerization, Colloid and Polymer Science. 284 (2006) 755-762.
[35] L. Wang, Y. Sun, J. Wang, J. Wang, A. Yu, H. Zhang, *et al.*, Preparation of surface plasmon resonance biosensor based on magnetic core/shell Fe3O4/SiO2 and Fe3O4/Ag/SiO2 nanoparticles, Colloids and Surfaces B: Biointerfaces. 84 (2011) 484-490.
[36] S. N. Abdollahi, M. Naderi, and G. Amoabediny, Synthesis and physicochemical characterization of tunable silica–gold nanoshells via seed growth method, Colloids and Surfaces A: Physicochemical and Engineering Aspects. 414 (2012) 345-351.
[37] L. Zhao, Y. Chi, Q. Yuan, N. Li, W. Yan, and X. Li, Phosphotungstic acid anchored to amino–functionalized core–shell magnetic mesoporous silica microspheres: A magnetically recoverable nanocomposite with enhanced photocatalytic activity, Journal of colloid and interface science. 390 (2013) 70-77.

[38] M. E. Khosroshahi and L. Ghazanfari, Synthesis and functionalization of SiO2 coated Fe3O4 nanoparticles with amine groups based on self-assembly, Materials Science and Engineering: C. 32 (2012) 1043-1049.
[39] S. H. Araghi, M. H. Entezari, and M. Chamsaz, Modification of mesoporous silica magnetite nanoparticles by 3-aminopropyltriethoxysilane for the removal of Cr (VI) from aqueous solution, Microporous and Mesoporous Materials. 218 (2015) 101-111.
[40] X. Zhang, H. Niu, Y. Pan, Y. Shi, and Y. Cai, Modifying the surface of Fe3O4/SiO2 magnetic nanoparticles with C18/NH2 mixed group to get an efficient sorbent for anionic organic pollutants, Journal of colloid and interface science. 362 (2011) 107-112.
[41] W. Li, B. Zhang, X. Li, H. Zhang, and Q. Zhang, Preparation and characterization of novel immobilized Fe3O4@ SiO2@ mSiO2–Pd (0) catalyst with large pore-size mesoporous for Suzuki coupling reaction, Applied Catalysis A: General. 459 (2013) 65-72.
[42] A. Walcarius, M. Etienne, and B. Lebeau, Rate of access to the binding sites in organically modified silicates. 2. Ordered mesoporous silicas grafted with amine or thiol groups, Chemistry of materials. 15 (2003) 2161-2173.
[43] A. Walcarius, M. Etienne, and J. Bessière, Rate of access to the binding sites in organically modified silicates. 1. Amorphous silica gels grafted with amine or thiol groups, Chemistry of materials. 14 (2002) 2757-2766.